Cessna 172 Research Task

Group 7651

Members:

Paul Shih: z5160958

Yash Kedar: z5184999

Amirul Fitri Mohamad: z5176959

Chao He: z5207818

Zheng (Roger) Luo: z5206267

Erik Mueller: z5209435

Abstract

This group assignment is composed to investigate the performance for wings' preliminary stress and stability for Cessna 172, in order to discover the reasons for its longevity and popularity within its class. Eventually, results can be obtained by adopting assumptions, clarifying fundamental loads and layout, employing MATLAB in order to solve the calculations, more importantly, by practicing the knowledge gained in this course. The analysis of the wings demonstrated the theoretically predicted trends based on solid mechanical principles and effectively demonstrates the effect of braces and spars on the stress distribution over wing of the aircraft. The fatigue life calculation yielded 3.8×10^4 *and* 3.4×10^4 cycles for the aircraft undertake off and cruising load conditions, respectively. The fatigue life calculation likely lacks accuracy as the values used for the calculations are largely approximated due to the lack of data on the stress oscillation over the aircraft's flight. More analysis is likely required to produce more accurate results.

Table of Contents

1. Introduction

The Cessna 172 Skyhawk is an American four-seat, single-engine, fixed wing aircraft. Which is one of most successful aircraft in history as the company had built more than 44000 units [1] since its first production in 1956. Due to its longevity and popularity, this group assignment is designed to perform the preliminary stress and stability analysis for wing of this particular aircraft - Cessna 172 in order to consolidate the knowledge gained in the course, in particular, stress distributions for critical structural members, margins of safety for yield, buckling and crippling, as well as the estimation of fatigue lives for critical structure have been investigated correspondently.

In order to explore the technical reasons such as its well accomplished design behind Cessna 172's longevity and popularity, its loads and layout have been examined at first, which include the simplify layout of aircraft, critical load cases, aircraft weight distribution, free body diagrams of wing, as well as other important load considerations, and the relationship between limit and ultimate load cases. These give a general understanding towards the aircraft, and which is necessary for analysing the wings' properties. Several important assumptions have to be made due to the existence of uncertainty and missing information, for example, the internal wing structure has been assumed based on cutaway drawings, and the thickness of the components have been assumed as which needs to consistent with the overall weight assumption. The critical wing station has been defined for the sake of calculations, and then the allowable buckling and crippling loads, internal stresses, margin of safety have been determined, as well as the fatigue life can be estimated by using S-N curve.

2. Analysis

2.1 Loads and Layout

Through identifying the possible critical loads, the act upon an aircraft during flight conditions, analysis of the Cessna 172 aircraft can be utilized to determine multiple aspects that include the maximum load before aircraft material yields and in understanding the stresses present in different flight scenarios

2.1.1 Layout of Aircraft

This section contains the structural diagrams of the Cessna 172 taken from [2].

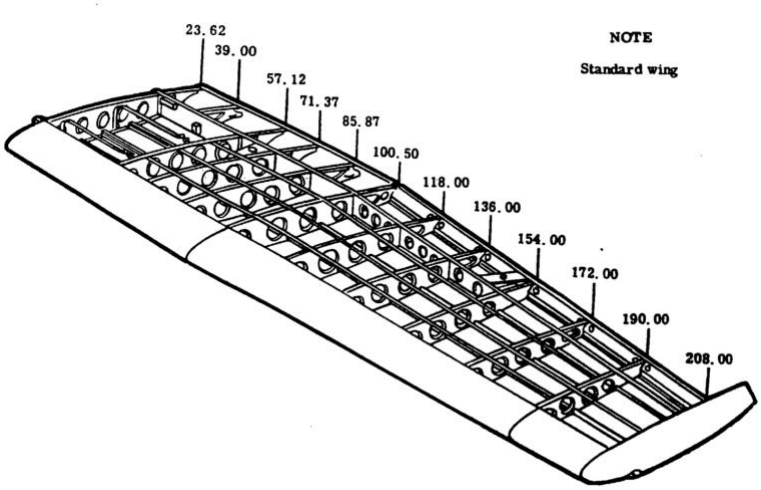

Figure 1. Standard Wing Dimensions

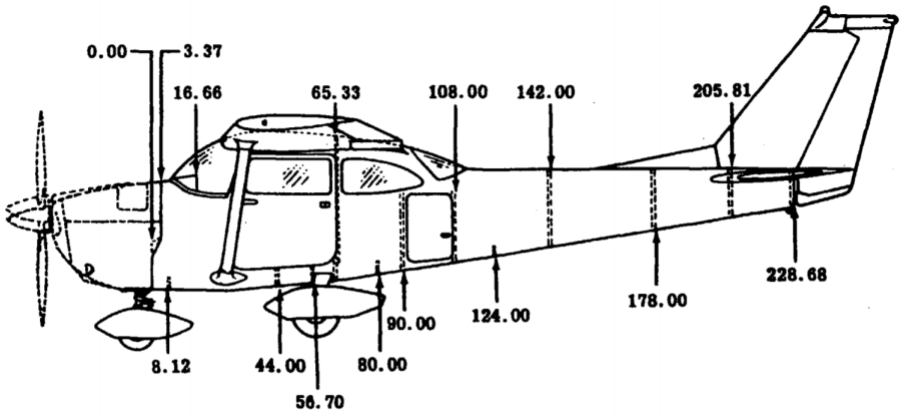

Figure 2. Cessna 172 Dimensions

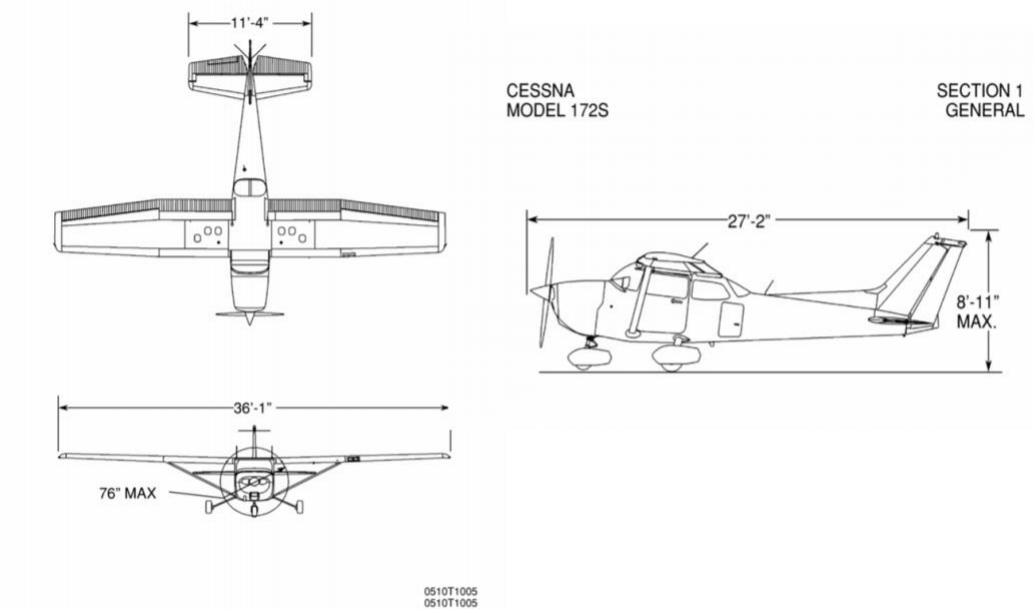

Figure 3. Cessna 172 Views

2.1.2 Critical Load Cases

During the service life of an aircraft, it experiences multiple flight and ground scenarios under varying loads. The analysis of all possible loads is near impossible due to significant possible variations across different cases, consequently, this report will focus on the analysis a few critical load cases including taxiing and takeoff of the aircraft. These cases are selected due to their relatively constant operation conditions. In the taxiing case, the weight of the aircraft is at the maximum contributed by the payload and the maximum fuel capacity. During takeoff, the lift generated is maximum to overcome the weight of the aircraft. The stress induced in different components of the aircraft, the wings in particular, is prominent and the taxiing and takeoff process are therefore selected as critical load cases for further analysis.

2.1.3 Aircraft Weight Distribution

Figure 4 below illustrates the force distribution on the Cessna 172 Skyhawk. Load weight and structural weight include multiple components and consists of the weight of the fuel, engines, wings of the aircraft, body of the structure, possible payloads and the tail of the Cessna 172 Skyhawk.

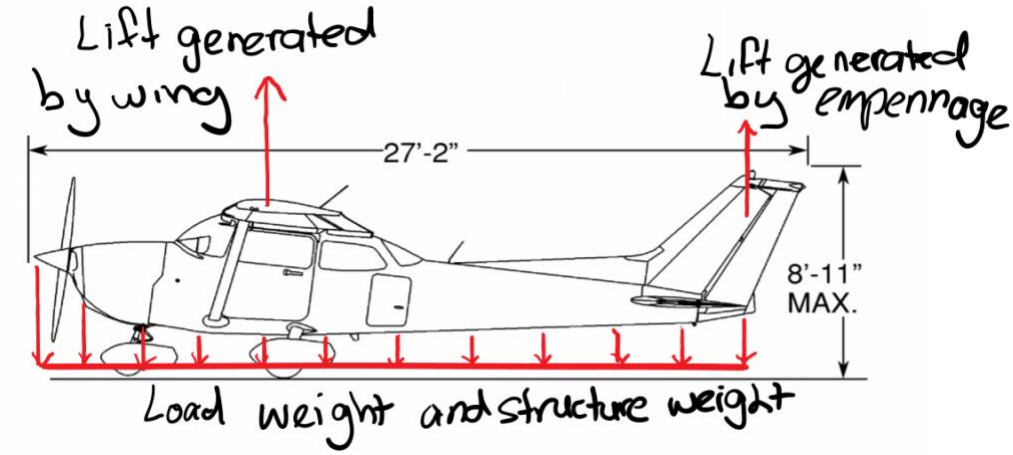

Figure 4. Weight Distribution

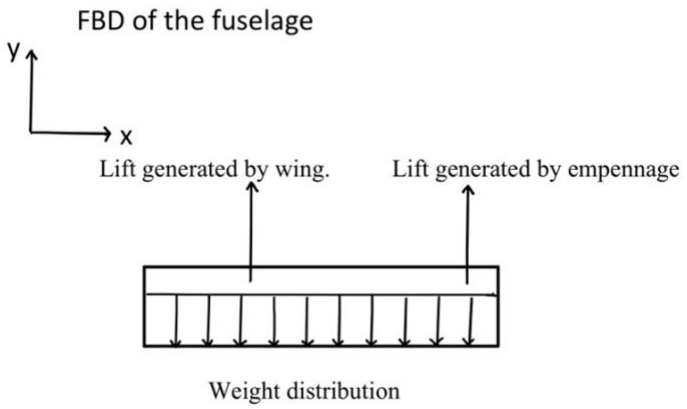

Figure 5. FBD of fuselage

2.1.4 Free Body Diagrams for wings for the load cases

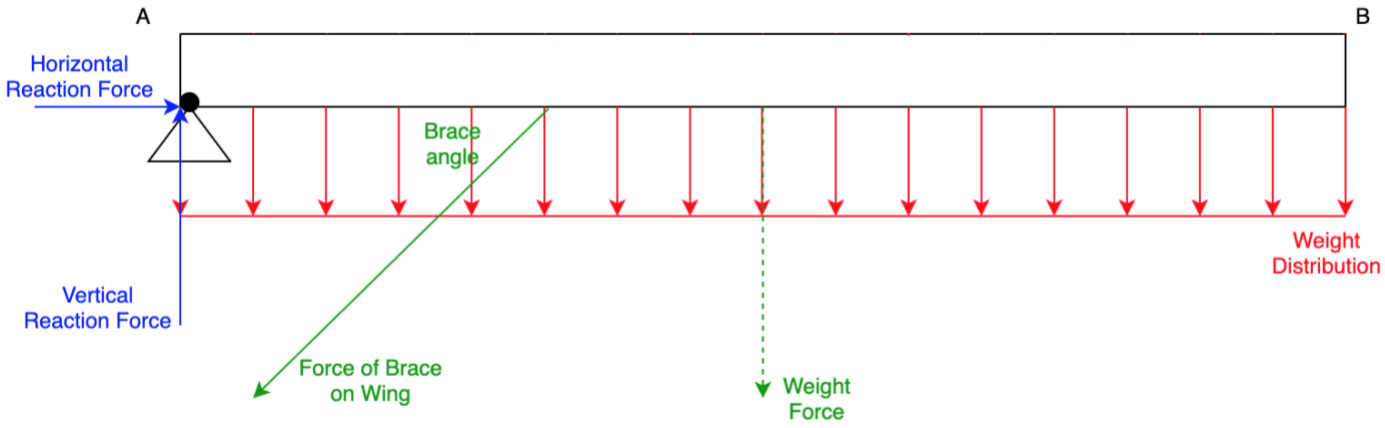

Figure 6: FBD of wings for load case 1 (taxiing)

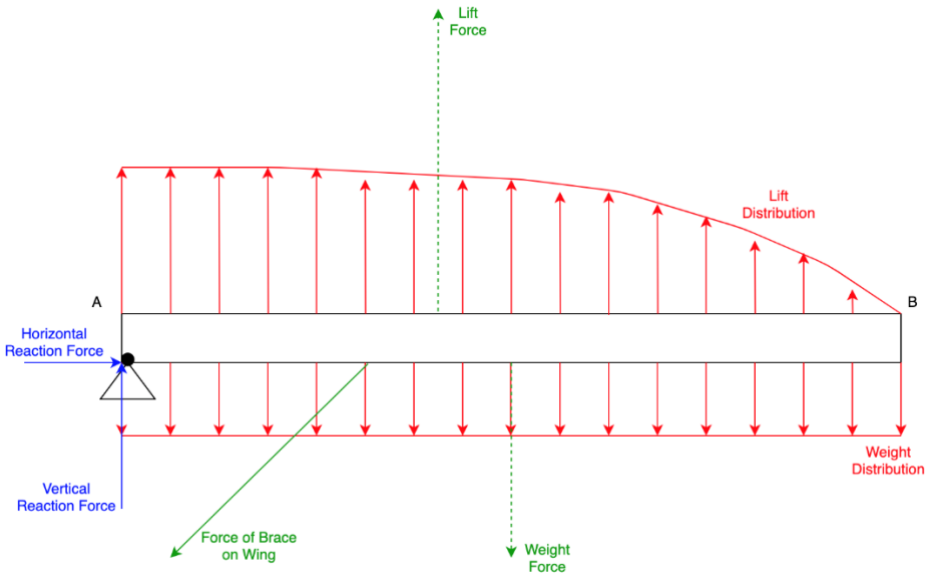

Figure 7: FBD of wings for load case 2 (during flight and take-off)

2.1.5 Important Load Considerations

The performance of the aircraft is affected by loads due to other components which should be considered during analysis. Weight concentration along the fuselage and the wings are not considered in the analysis as a uniform weight distribution is assumed to simplify calculations. These includes significant weight contributions such as the engine (approximate dry weight of 269 pound), ribs throughout the aircraft's structure, passengers and payloads which would all contribute to inaccuracies in the calculations. The fuel tank is located within the wing structure at position 2 in Figure 8 and has a fuel capacity of 42 gallons where 38 gallons are usable. Fuel consumption during flight will therefore cause gradual shifts in the weight distribution across the aircraft's neutral axis during cruising but will have little impact during the critical load cases examined in this report (taxing and take off) as relatively little fuel is consumed during both processes.

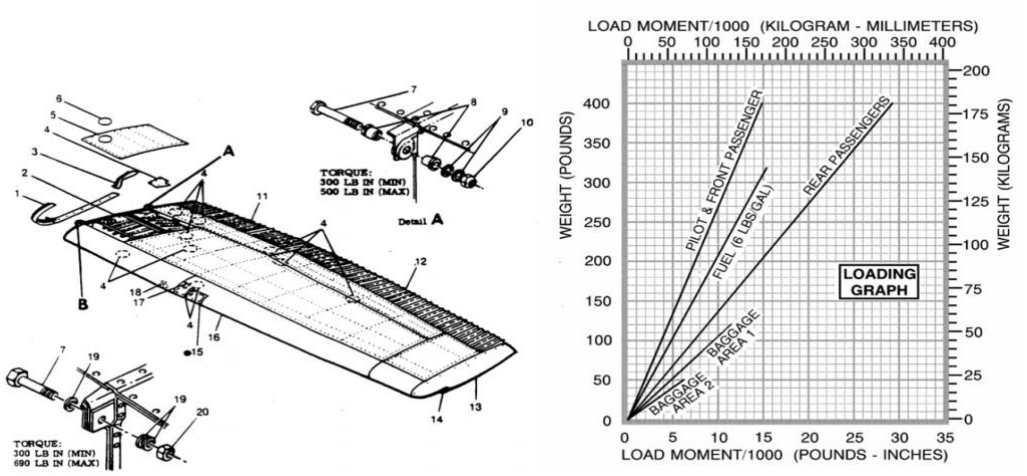

Figure 8. Cessna 172

With respect to the analysis of the two critical loads selected, there are also many other aircraft loads that should be considered due to their essentiality to the design cycle but are not further analysed throughout the report. However, by discovering the different types of loads acting on the aircraft early, it reduces the expense and risk of having to potentially restart design process to cater for the possible loads. An aircraft experiences dynamic and static loads, maneuvering throughout flight, flight envelope and loading of payload scenarios, contributing to the vast amount of loading conditions.

The possible loads that an aircraft may experience corresponds with the requirements specified by aircraft project and the airworthiness, which determines the load cases that should be considered during the design process. Airworthiness generally dictates the ground and flight conditions that affect the structural integrity of the aircraft through load analysis, analysis of mission profile and simulations. The specification requirements of aircraft project mainly centers around public and military regulations and the main purpose of the aircraft design, whether the focus is either speed related or transfer of payload.

Through the combination of the multiple aspects of project requirements and airworthiness that contribute to the load generation, all possible loadings that act upon the aircraft during varying scenarios that covers the operational envelope and the flight regime of the aircraft can be accounted for. Different load cases can include flap configurations, temperature, altitudes, airspeeds, mass states, thrust levels, flight and ground conditions.

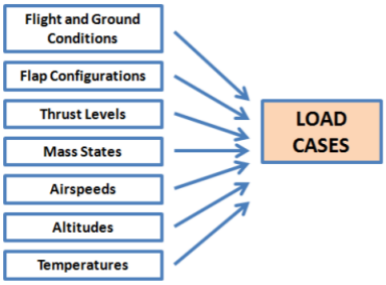

Figure 9. Load Cases

2.2 Airspeeds

Airspeeds are important factors in determining possible loads and are also known as "V-Speeds". As the majority of ground and flight conditions are defined with the airspeeds, it is extensively used during load analysis. There are distinct types that stem from airspeeds and these include:

Stall Speed (denoted as V_S)

- The stall speed is the minimum velocity of the aircraft to remain at level flight. The stall speed is dependent on factors related to the aircraft's altitude, mass and acceleration.

Cruise Speed (denoted as V_C)

- Cruise speed ranges for different aircraft and are based on their respective certification regulations. Generally, it is defined as the velocity that is required for an aircraft to remain at the cruising phase, leveling of the aircraft at a set altitude usually after climb and before descent of commercial aircrafts.

Maneuver Speed (denoted as V_A)

- Maneuver speed is the airspeed limitation for an aircraft to fly with maximum load factor. Velocities higher than the maneuver speed will cause detrimental deformations of the aircraft when at deflection of flight control surface.

Dive Speed (denoted as V_D)

- Dive speed is the maximum speed that should not be exceeded when aircraft dives.

Gust Speed (denoted as V_B)

- Gust speed is an external factor accounted for and is defined as the airspeed that relates to the intensity of maximum gust.

Maximum Speed (denoted as V_H)

- The speed required for level flight in regard to power being continuously supplied.

The flight regime of a specific aircraft is established with the altitude and airspeeds and are plotted on a V-A diagram, as shown in Figure 10, dictating the conditions experienced and results in load cases during flight of aircraft.

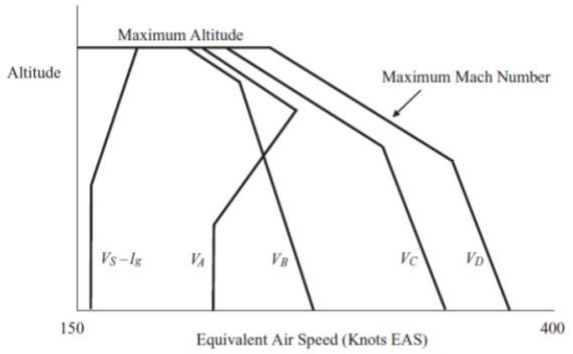

Figure 10. V-A Diagram

2.3 Load Factor and V-n Diagrams

Load factor as a design parameter contributes greatly to load cases as it dictates the aerodynamic force and gross weight ratio of an aircraft. It is also considered as any applied force that causes deviation upon the flight path of an aircraft. Thus, aircrafts are designed to resist a specific or maximum load factor, preventing material yield and preventing structure deformation. Gust maneuver in turbulent air also affects load factor and are cases of load on the aircraft. The relationship between load factor and airspeed illustrate a fight envelope, also known as V-n diagram as shown in Figure 11.

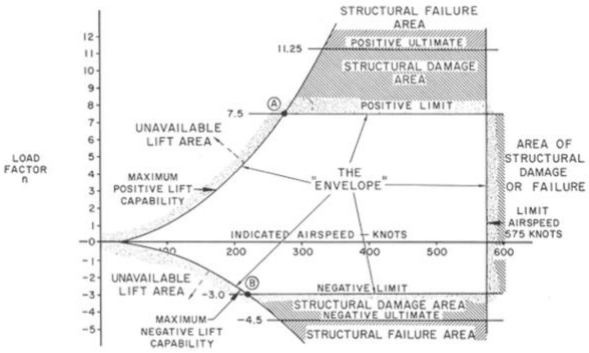

Figure 11. V-n Diagram, credit from [3]

2.4 Weight Envelopes and Mass States

Load analysis is executed for combined loads such as payload, aircraft fuel capacity and the number of passengers onboard. The possible combinations are known as mass states and represent specific weights that include Maximum Landing Weight (MLW) and Maximum Take-off Weight (MTW). The weight envelop dictates the relationship between weight of aircraft and the center of gravity and is illustrated in Figure 12.

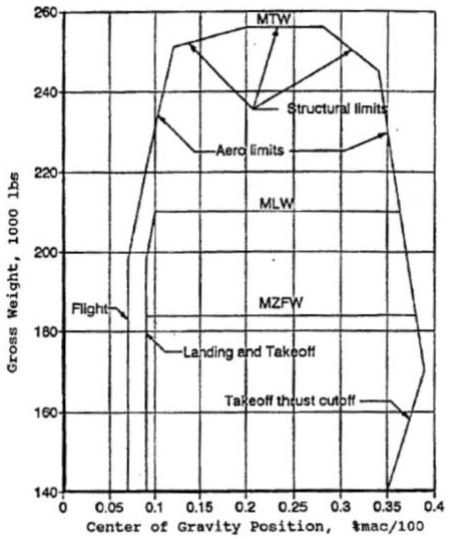

Figure 12. Weight Envelope

2.5 Flight Conditions

Flight conditions are major load cases and are generally based upon the specifications of airworthiness with respect to military or civilian use. However, the design project requirements may specify additional maneuvers and are thus analysed respectively. Flight loading cases comprises of different maneuvers.

2.5.1 Maneuvers

Symmetric Maneuvers

Symmetric maneuvers, observed in Figure 13, consist of pitching maneuvers and pull up and push down maneuvers and may expose aircrafts to critical loads. Abrupt situations such as sudden pull up after stall recovery or at excessive diving speed will cause critical loads to be implicated upon the structures of the aircraft such as the horizontal tail for pitch maneuver load conditions.

Rolling Maneuvers

Rolling maneuvers, observed in Figure 13, causes maximum deflection in the ailerons. The ailerons are used for rolling maneuvers for performance aircrafts and used as well in commercial jets, better known as a turn or rolling motion. The aileron caused one tip of the wing to move down and one to move up. This banking motion induces a side force component that is unbalanced and thereby causes a curve in the flight path of the aircraft. This unbalanced force is a critical load and induces large amounts of stress on different components of the aircraft.

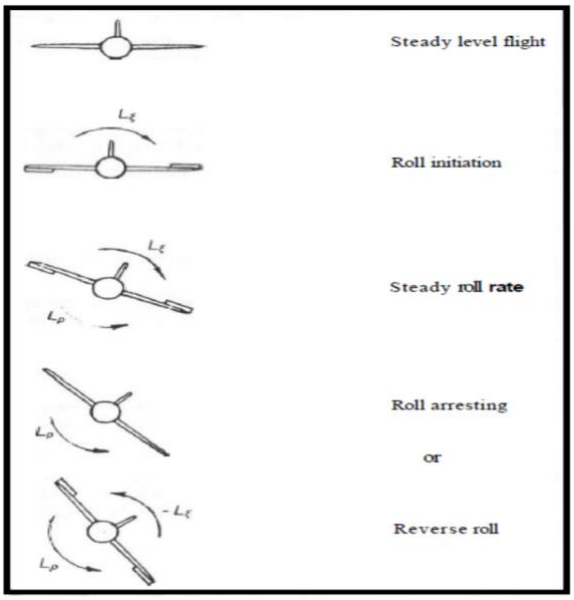

Figure 13. Manoeuvres

2.5.2 Grounds conditions

In respect to ground conditions, structures of the aircraft such as local components of the landing gear and fuselage components are affected greatly by the critical load cases. Ground conditions can be separated into different sub-categories and encompasses landing, taxiing and ground handling loads.

Landing

Landing conditions are detailed and analysed with airworthiness specifications. Figure 14 demonstrates various specified ground conditions.

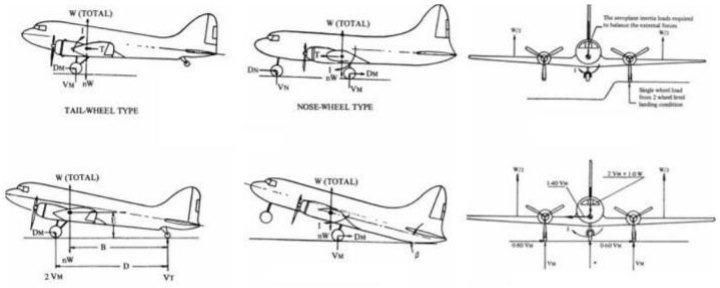

Figure 14. Landing Conditions

Taxiing

Similarly, taxiing conditions, which include ground turning, pivoting and braking, are specified in airworthiness specifications.

Ground Handling Loads

Ground handling loads consists of three different sub-categories comprising of towing, mooring and jacking.

Limit and Ultimate Load Cases

The difference between limit and ultimate load cases is that limit is the actual and possible load and ultimate is a hypothetical load. The limit load case refers to the maximum loads that are to be encountered during an aircraft's service flight. This takes into account of all possible loads such as the entire aircraft with its passengers and payloads. The aircraft must support these loads and must not cause permanent and detrimental deformations, where stresses are maintained

below yield point. Whereas the ultimate load is considered the worst-case scenario whereby the limit load (maximum for safety reasons) is multiplied by the factor of safety. This occurs when

$$Ultimate\ Load = Limit\ Load \times Factor\ of\ Safety \tag{2.5.1}$$

The reason being that it provides more precautions as such is needed for vehicles that travel at high altitudes, where the unexpected happens. This ultimate load accounts for unexpected factors such as increase in non-intentional external loads like forces from emergency landing and possible high wind velocities during takeoff and landing. As per regulations the factor of safety unless otherwise stated is to be taken as 1.5.

2.6 External Loads, Shear and Bending Moments

The Cessna 172 Skyhawk is an aircraft with a high-mounted wing and a diagonal brace joining the bottom of the fuselage with the wing about a third of the way from root to tip. Due to the nature of metal structures, there will be a higher level of deflection at the mid-wing than at the wing root, resulting in the diagonal brace taking the majority of the lift and weight moments, instead of the cantilever at the root. Since the moment at the wing root will be comparatively small, a hinge joint assumption was made. Another assumption made was that the total wing construction was 15% of the mass of the total weight. To better illustrate the forces present along the span, a Free Body Diagram (FBD) was constructed:

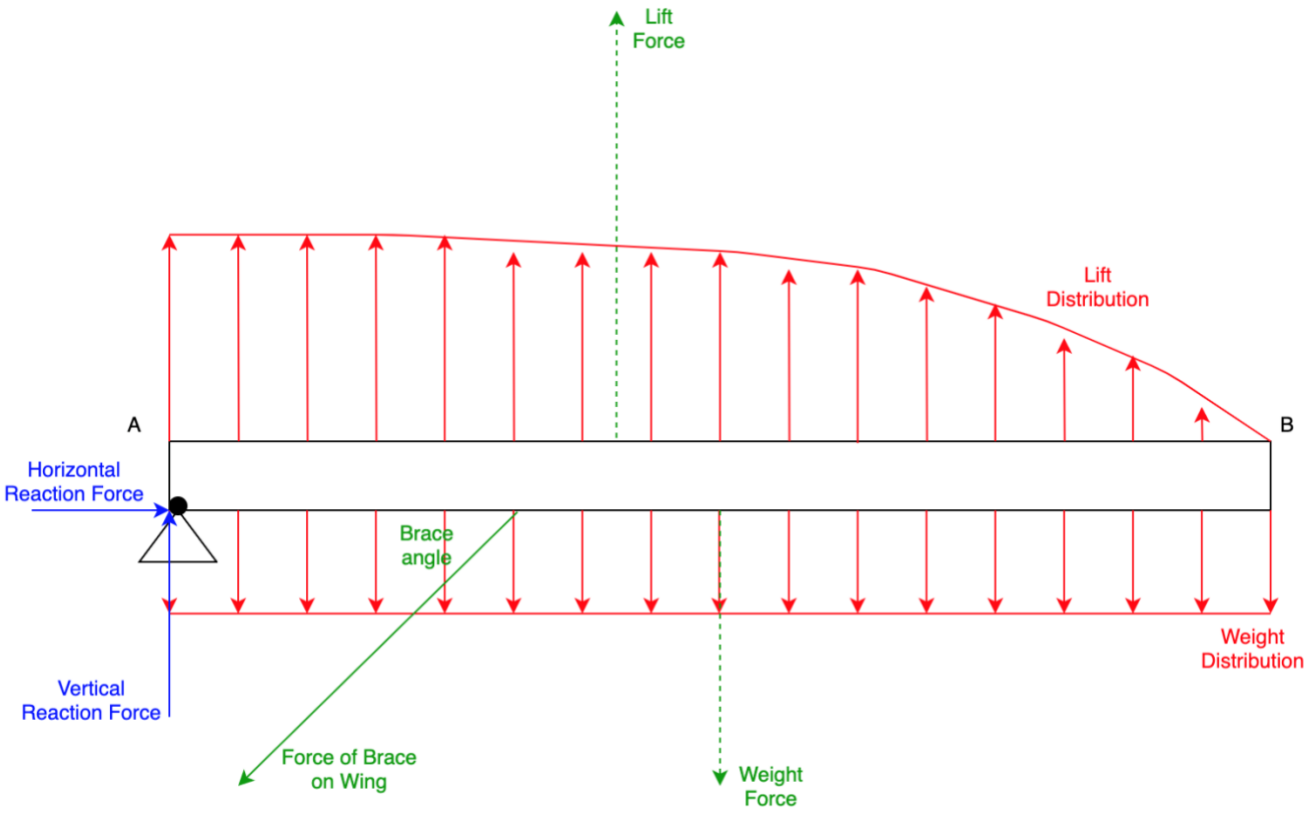

Figure 15.Free Body Diagram of a wing in Steady Flight

To find the force, shear and bending moment as a function of length along the wing, it is possible to ignore the complicated internal geometry of the wing and do a simple slender beam analysis, but before a beam analysis is carried out, the lift and weight distribution – and their resultant point loads and locations must be calculated.

2.6.1 Distributed Loads

The lift distribution is not constant along the wing: It decreases in a nonlinear fashion towards the outboard due to both a wing taper and wingtip vortex interactions – in fact, the lift is effectively zero at the wingtip since there are no winglets or similar devices. For this analysis, a Schrenk's Distribution was used as the approximation for lift as a function of span length, and hence a constant lift distribution is assumed initially:

$$l = \frac{L}{b} = \frac{n * W}{b} = \frac{n * m * g}{b} \tag{2.6.1}$$

Where $l = constant\ lift\ distribution\ (Nm^{-1}), L = lift\ (N), b = total\ wingspan\ (m), n = load\ factor, m = total\ aircraft\ mass\ (kg)$ and $g = 9.81\ ms^{-2}$.

Schrenk's distribution takes a constant force distribution and fits a quarter ellipse as a function of wing length (x) such that they both have the same area. This comes out as:

$$y = \frac{1}{2}\left(\left[\frac{16 * l^2}{\pi^2} - \frac{64 * l^2 * x^2}{\pi^2 * b^2}\right]^{0.5} + l\right) \tag{2.6.2}$$

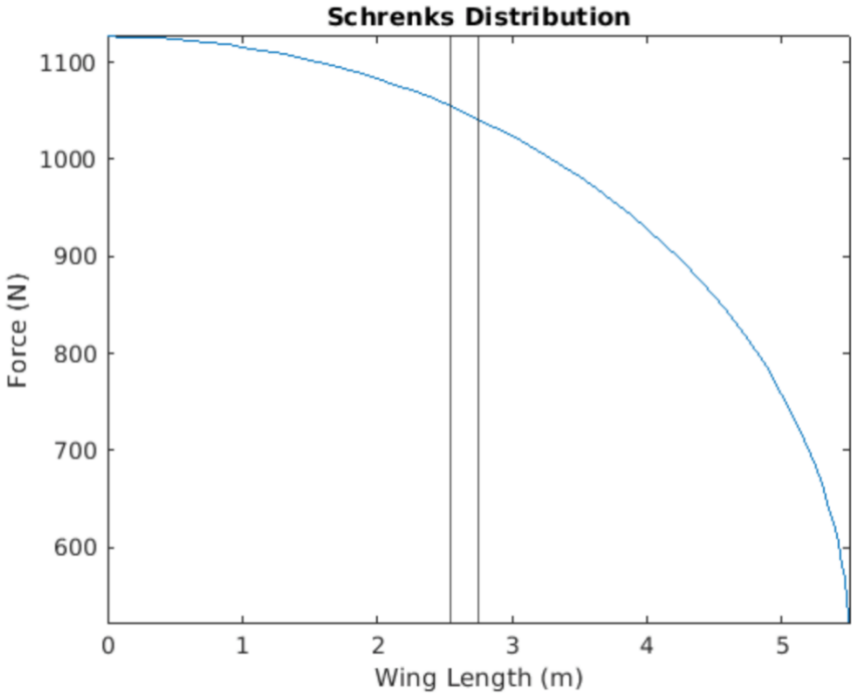

Figure 16. Schrenk's Distribution

The total lift force acting upwards can be calculated by integrating, and the centroid of this distribution is also calculated by integrating:

$$L = \int_0^{\frac{b}{2}} y * dx = \int_0^{\frac{b}{2}} \frac{1}{2}\left(\left[\frac{16 * l^2}{\pi^2} - \frac{64 * l^2 * x^2}{\pi^2 * b^2}\right]^{0.5} + l\right) dx \tag{2.6.3}$$

$$\bar{x}_{lift} = \frac{\int_0^{\frac{b}{2}} x * y * dx}{\int_0^{\frac{b}{2}} y * dx} = \frac{\int_0^{\frac{b}{2}} x * \frac{1}{2} * \left(\left[\frac{16 * l^2}{\pi^2} - \frac{64 * l^2 * x^2}{\pi^2 * b^2}\right]^{0.5} + l\right) dx}{\int_0^{\frac{b}{2}} \frac{1}{2}\left(\left[\frac{16 * l^2}{\pi^2} - \frac{64 * l^2 * x^2}{\pi^2 * b^2}\right]^{0.5} + l\right) dx} \tag{2.6.4}$$

The total wing weight is assumed to be 0.15 times the total aircraft weight, and is assumed to be in a constant weight distribution (in the spanwise direction) since the wing ribs are a relatively small mass concentration compared with the spanwise mass distribution of the wing structural components:

$$W_{wing} = 0.15 * n * \frac{W}{2} \tag{2.6.5}$$

$$w_{wing} = \frac{W_{wing}}{0.5 * b} \tag{2.6.6}$$

$$\bar{x}_{weight} = 0.25 * b \tag{2.6.7}$$

2.6.2 Reaction Forces and Forces Due to the Wing Brace

Sum of moments around the wing root is used to calculate the force of the brace on the wing:

$$\sum M_A = L * \bar{x}_{lift} - W_{wing} * \bar{x}_{weight} + F_{brace} * b_{brace} * sin(\theta_{brace}) = 0$$

$$F_{brace} = -\frac{\left(L * \bar{x}_{lift} - w_{wing} * \bar{x}_{weight}\right)}{b_{brace} * Sin(\theta_{brace})} \tag{2.6.8}$$

Reaction forces at the wing root are calculated using the vertical and horizontal force equilibrium:

$$\sum F_{vertical} = L + F_{brace} * sin(\theta_{brace}) - W_{wing} + R_y = 0$$

$$R_y = -\left(L + F_{brace} * sin(\theta_{brace}) - W_{wing}\right) \tag{2.6.9}$$

$$\sum F_{horizontal} = +F_{brace} * cos(\theta_{brace}) + R_x = 0$$

$$R_x = -F_{brace} * cos(\theta_{brace}) \tag{2.6.10}$$

2.6.3 Shear Force and Bending Moment Diagrams

The loading function of the vertical forces is used to determine the shear forces and bending moment in that direction:

$$F_y = y - w_{wing} + F_{brace} * sin(\theta_{brace}) * \delta(x - b_{brace}) \tag{2.6.11}$$

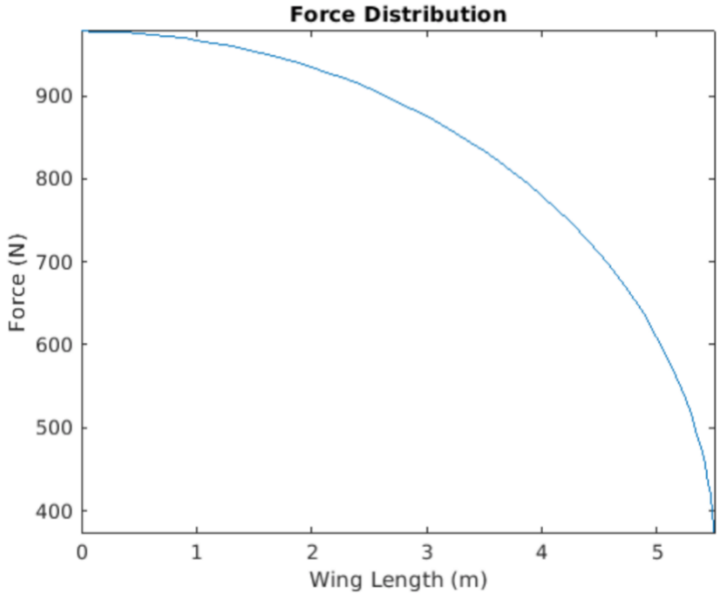

Figure 17. Shear Force Distribution on the Wing

The shear force as a function of wing length (x) can therefore be found by integrating the loading function, and this can then be graphed to create a Shear Force Diagram (SFD):

$$S_y = \int F_y\,dx\ + R_y = \int \left(y - w_{wing} + F_{brace} * sin(\theta_{brace}) * \delta(x - b_{brace})\right) dx + R_y \tag{2.6.12}$$

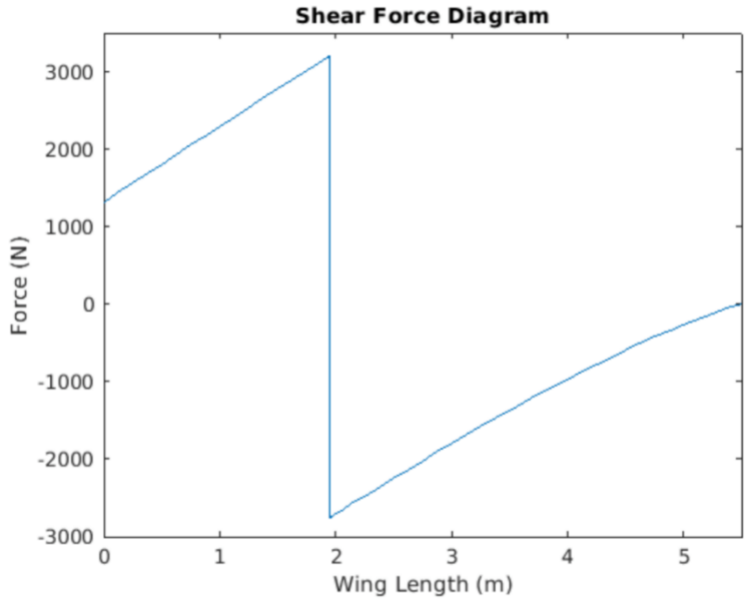

Figure 18. Shear Force Diagram of the wing

The bending moment as a function of wing length (x) can be calculated by integrating the shear force function, and this can be graphed to create a Bending Moment Diagram (BMD):

$$M_y = \int S_y\,dx = \iint \left(y - w_{wing} + F_{brace} * sin(\theta_{brace}) * \delta(x - b_{brace})\right) dx \tag{2.6.13}$$

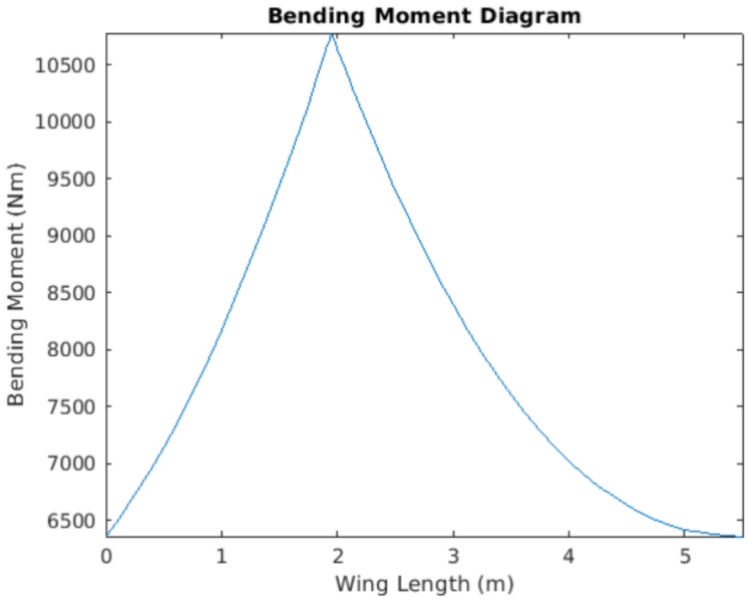

Figure 19. Bending Moment Diagram for the Wing

2.6.4 Ground Loading

Sum of moments around the wing root is used to calculate the force of the brace on the wing:

$$\sum M_A = -W_{wing} * \bar{x}_{weight} + F_{brace} * b_{brace} * sin(\theta_{brace}) = 0$$

$$F_{brace} = -\frac{(-w_{wing} * \bar{x}_{weight})}{b_{brace} * Sin(\theta_{brace})} \tag{2.6.14}$$

Reaction forces at the wing root are calculated using the vertical and horizontal force equilibrium:

$$\sum F_{vertical} = F_{brace} * sin(\theta_{brace}) - W_{wing} + R_y = 0$$

$$R_y = -\left(F_{brace} * sin(\theta_{brace}) - W_{wing}\right) \tag{2.6.15}$$

$$\sum F_{horizontal} = +F_{brace} * cos(\theta_{brace}) + R_x = 0$$

$$R_x = -F_{brace} * cos(\theta_{brace}) \tag{2.6.16}$$

On the ground, the wings do not generate lift and therefore the loading function is:

$$F_y = -w_{wing} + F_{brace} * sin(\theta_{brace}) * \delta(x - b_{brace}) \tag{2.6.17}$$

And therefore:

$$S_y = \int F_y\, dx + R_y = \int \left(-w_{wing} + F_{brace} * sin(\theta_{brace}) * \delta(x - b_{brace})\right) dx + R_y \tag{2.6.18}$$

$$M_y = \int S_y\, dx = \iint \left(y - w_{wing} + F_{brace} * sin(\theta_{brace}) * \delta(x - b_{brace})\right) dx \tag{2.6.19}$$

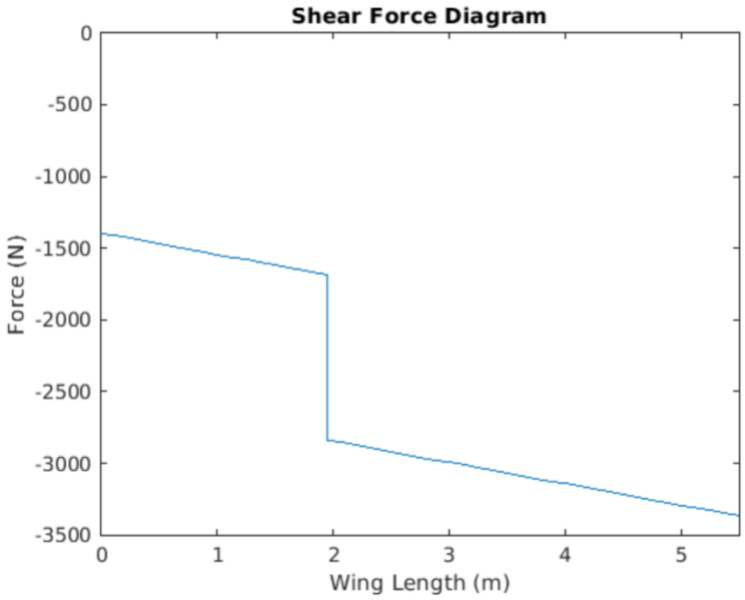

Figure 20. Shear Force Diagram of Wing in Ground Loading

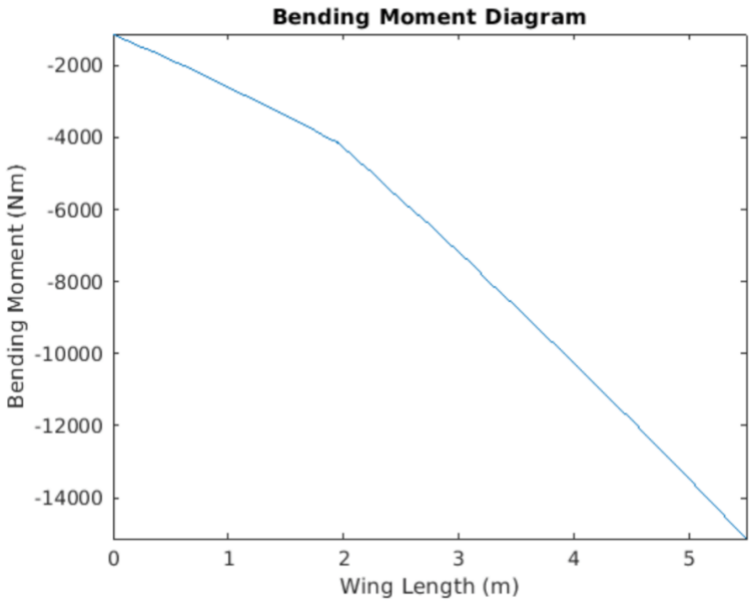

Figure 21.Bending Moment Diagram of wing in Ground Loading

2.7 Wing Deflection:

Since the bending moment equation has been calculated, and the second moment of area coming from the wing idealization (discussed in later sections), it is possible to calculate the slope and deflection of the wing:

$$\frac{d\theta}{dx} = \frac{1}{E * I_{xx}} \int M_y \, dx = \frac{1}{E * I_{xx}} * f(x) + C_1 \tag{2.7.1}$$

The fixed anchor point from the previous analysis suggests that the slope is zero at the wing-brace joint location:

$$C_1 = -\frac{1}{E * I_{xx}} * f(b_{brace}) = -\frac{d\theta}{dx}(b_{brace}) \tag{2.7.2}$$

Deflection is one integral step further:

$$V = \frac{1}{E * I_{xx}} \iint M_y \, dx = \frac{1}{E * I_{xx}} * f(x) = \frac{x}{E * I_{xx}} * f(b_{brace}) + C_2 \tag{2.7.3}$$

Deflection is zero at wing joint:

$$C_2 = V(0) = -\frac{0}{E * I_{xx}} * f(b_{brace}) = 0 \tag{2.7.4}$$

Aircraft in cruise:

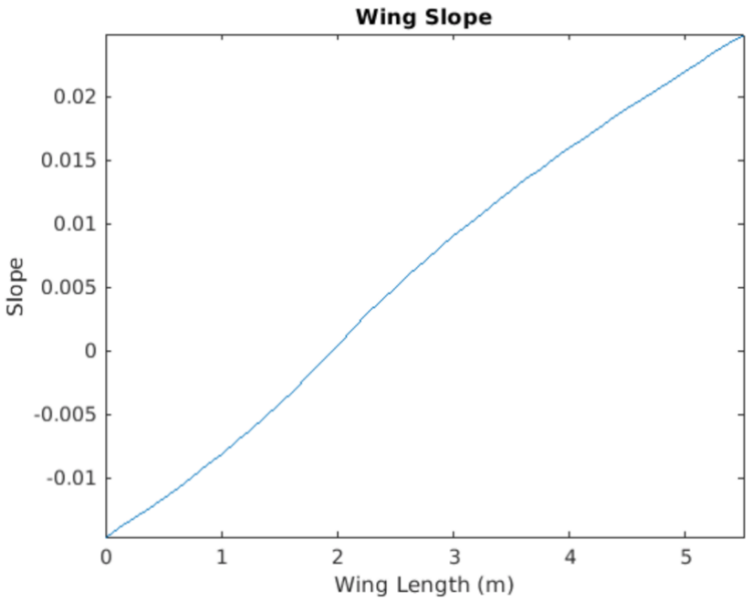

Figure 22. Wing Slope when aircraft in Cruise

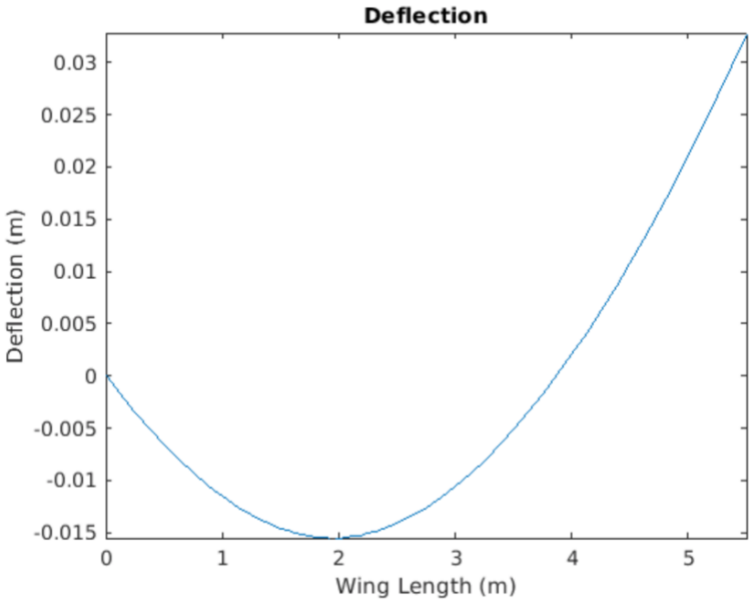

Figure 23. Tip deflection when aircraft in Cruise

On the ground:

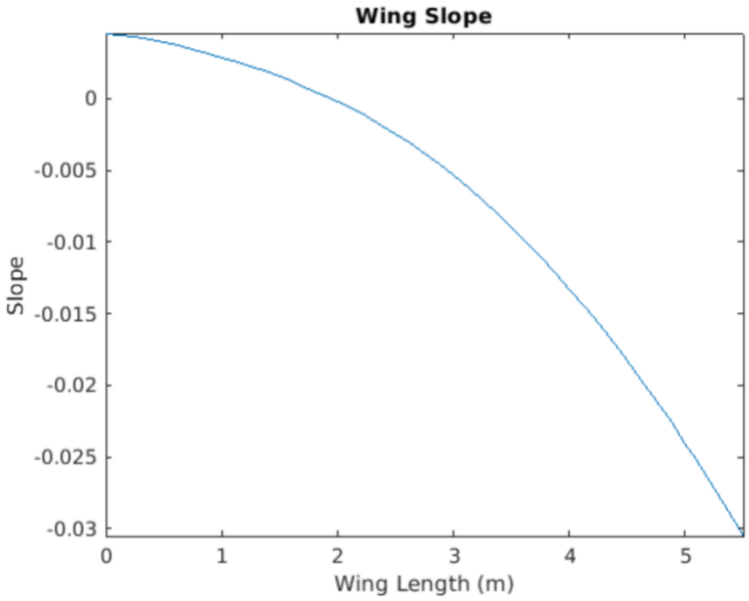

Figure 24. Wing Slope when aircraft on Ground

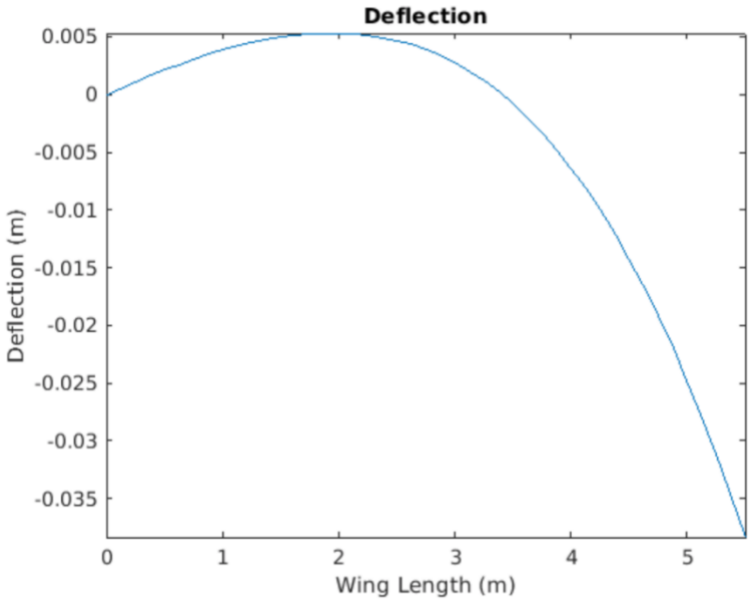

Figure 25. Tip Deflection when aircraft on ground

2.7 Wings

2.7.1 Define a simplified cross-section

The cross-section of the wing root of a Cessna 172 was found to be a NACA 2412 modified airfoil. Due to the absence of any publicly available documents for the specifications of the airfoil, a rough analysis was done on the chord length by scaling, and the coordinates for the same were taken from airfoil tools [4] .The simplified airfoil cross section is illustrated in Figure 26 below.

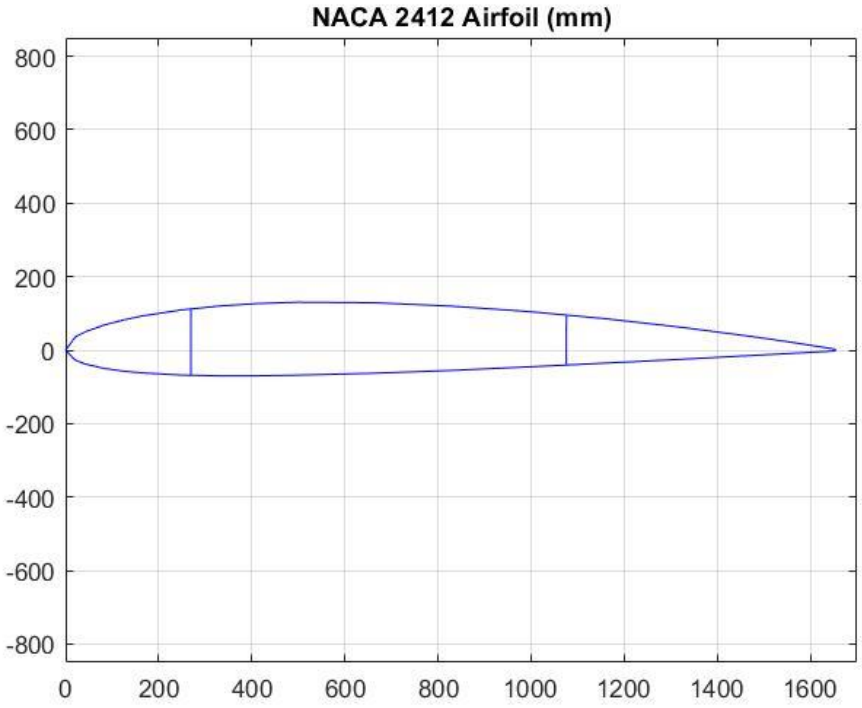

Figure 26. NACA 2412 Airfoil with Front and Rear Spars

An estimate of the Spar locations was made and incorporated in the airfoil plot. Figure 26 displays the wing profile and the location of the spars. A total of 6 stiffeners were found to be attached to the skin. Since the wing includes ailerons behind the Rear Spar, which are detached from the actual wing, these were discarded in the idealisation for the cross-section.

Table 1 below is the record of the approximation of the wing root cross-section. The locations of the Front and Rear Spar mentioned are taken from the leading edge

Table 1. Dimensions of Materials in the Cross-section

Chord length (m)	1.66
Skin thickness (mm)	0.813
Front spar location (mm)	270
Front spar thickness (mm)	2.00
Front spar length (mm)	192
Rear spar location (mm)	1080
Rear spar thickness (mm)	2.00
Rear spar length (mm)	121

2.7.2 Idealialisation

The cross-section was idealised into 12 booms and 12 panels. The quantity and location of the booms were selected based on the number of nodes (skin – spar, skin – stiffener intersection) on that cross-section. Figure 27 below is a representation of the idealised cross-section

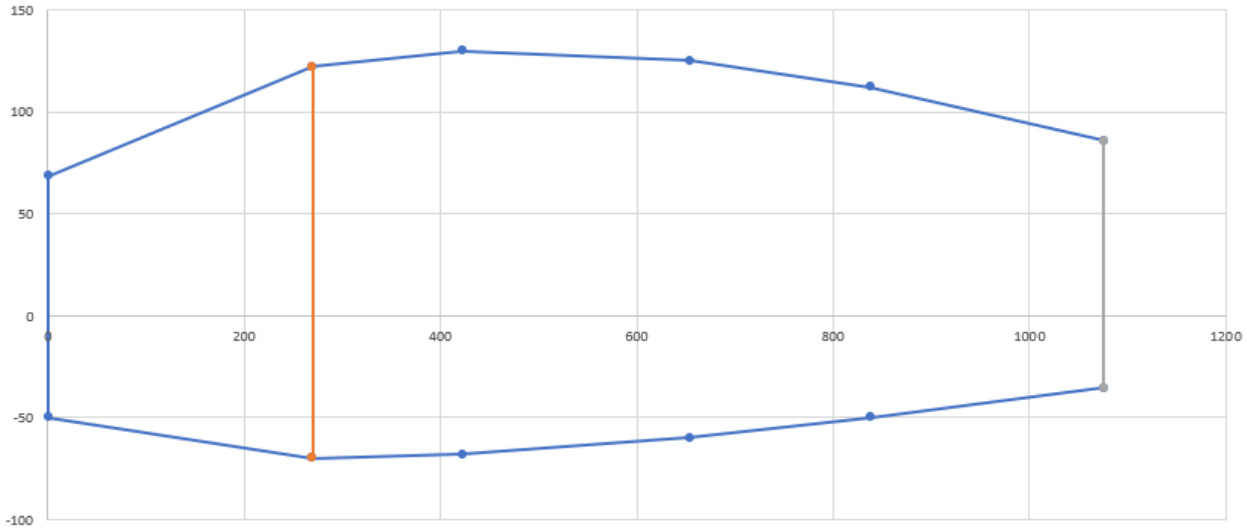

Figure 27. Idealised Wing Cross-section

2.7.3 The allowable Buckling and Crippling loads for each Skin Panel and Stiffener Section

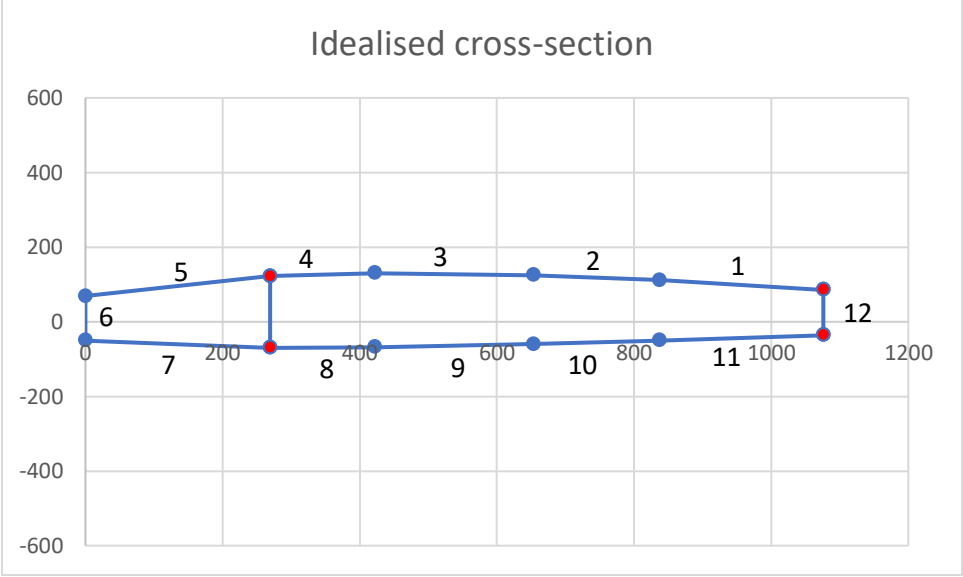

Figure 28. Idealised cross-section for buckling and crippling analysis, showing idealised stiffeners location

In the analysis of buckling and crippling condition for the wing root section, the cross-section of the internal wing structure needs to be simplified in order to carry out the calculation. Idealised wing section in Figure 28 has all the booms located at the points where hat-shaped stiffeners are lined up along the wing, except at the points marked red in the figure where the support also comes from the front and rear spar. The panels are going to be labelled by numberings as shown in the figure above to ease the analysis and the stiffeners labelling are the same as the panels it preceeds. The main purpose of

stiffeners is to prevent the wing skin from bending although it also has significant effect on the overall strength of the wing cross-section to resist buckling and crippling.

In the wing structure, allowable buckling and crippling loads for each skin panel and stiffener section are important. For the convenience of calculation, the material of stiffener has been assumed same as the material applied on the skin, which is 2024-T3 Aluminium. The material properties were shown in Table 2.

Table 2.Material properties of AL2024

Compressible young's modulus (E_c)	73.77 GPa
Poisson ratio	0.33
Compressive yield strength (F_{cy})	276 Mpa

The compressible buckling and the shear buckling were both acting on the wing structure.

The allowable compressible buckling for each skin panel was calculated by the following equation:

$$\sigma_{Cr} = \frac{\pi^2 * K_c * E_c}{12(1-\mu^2)} * \left(\frac{t}{b}\right)^2$$

Eq. 1. Compressible buckling formula

Where K_c was found in compression buckling stress coefficient diagram, Figure 29.

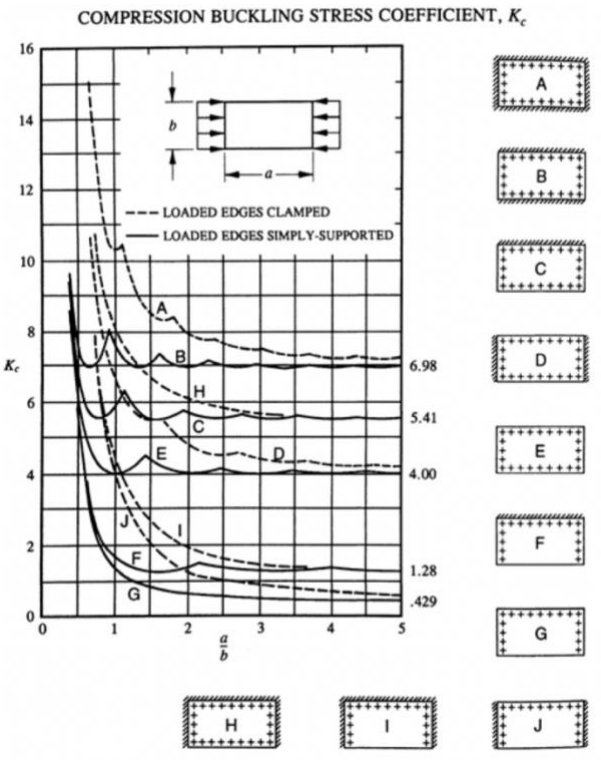

Figure 29. Compression buckling coefficient.

In order to use Figure 29, an assumption on the wing geometry was made where the curvature of the skin around the wing cross-section considered negligible, resulting in a flat surface with zero curvature parameter. To determine the value of K_C, the condition of the skin in terms of how it was being supported around the wing structure had to be known.

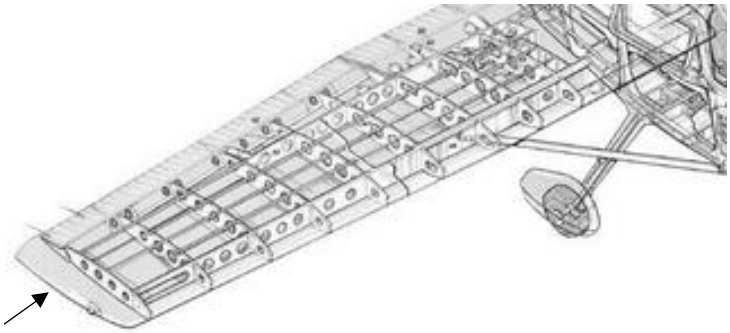

Figure 30. Internal wing structure

From Figure 30Figure 31, each section of skin is separated and simply supported by pairs of ribs on the loading edge marked by an arrow and 'clamped' at the adjacent sides by stiffeners traversing along the wing.

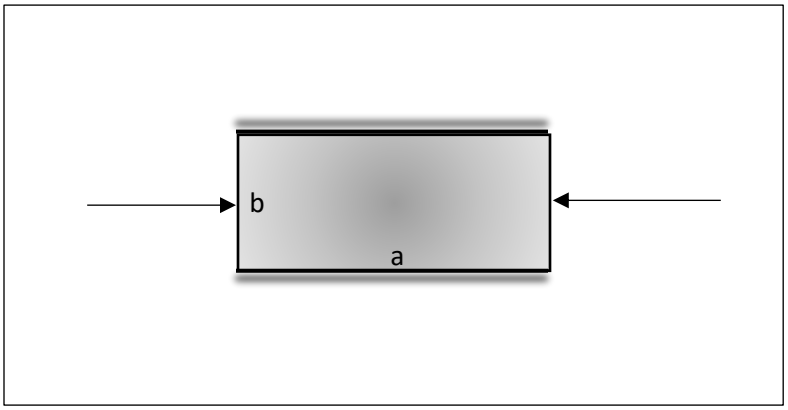

Figure 31.Skin section

Figure 31 shows an enlarged image of how the skin section was loaded at the simply supported edge and clamped at the unloaded edge, making the buckling condition B on Figure 29. The compression buckling coefficient was found by calculating the aspect ratio of the skin section and extracting the K_C value from the B plot.

$$Aspect\ ratio = \frac{a}{b}$$

The a values were found by calculating the distance between each ribs, assuming each ribs were separated evenly across the length of the wing while b values were found by calculating the distance between adjacent stiffeners.

Table 3.Aspect Ratio of every Skin Panel for Condition B

Panel	Distance, b (mm)	Aspect Ratio
1	240.2	2.5
2	184.4	3.3
3	230.8	2.6
4	153.2	3.9
5	274.6	2.2
6	118.1	5.1
7	270.0	2.2
8	153.2	3.9
9	230.9	2.6
10	184.1	3.3
11	239.2	2.5
12	121.1	5.0

Based on the table above, the smallest value for aspect ratio was 2.2 which in the compression buckling stress coefficient graph (Figure 29), the B plot has already converged closer to 6.98. Hence it can be approximated that the all the skin panel has K_C values of 6.98.

There are 3 different types of stiffeners used in the design of this wing. The first one being the extruded hat-shaped stiffener as shown in Figure 32 below

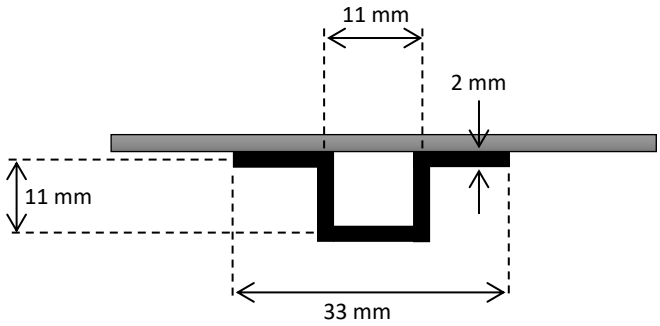

Figure 32. Hat-shaped stiffener dimensions

Another type of stiffener was used in the design of the front spar that acted as the front spar cap, Figure 33, and in the design of rear spar that acted as the rear spar cap, Figure 34.

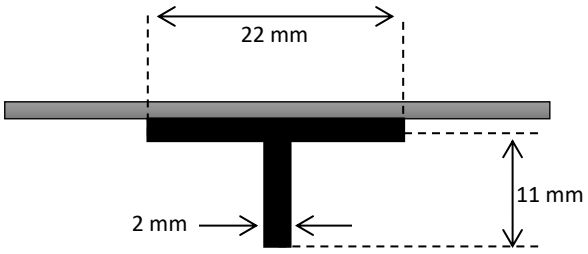

Figure 33. Front spar cap dimensions

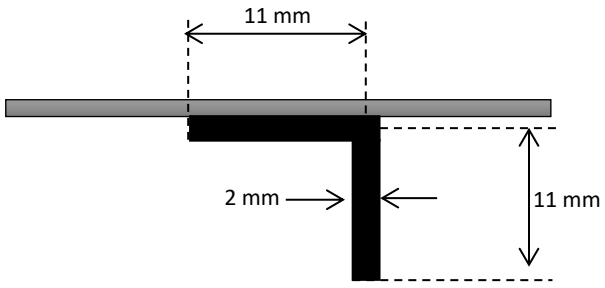

Figure 34. Rear Spar cap dimensions

Applying thin-walled assumption, the calculation of the individual and combined skin and stiffener's geometrical properties necessary for analysis such as the area, critical crippling stress (F_{cc}) and effective width (W_e) became much easier.

$$F_{cc} = \begin{cases} \dfrac{c_e\sqrt{F_{cy}E_{cc}}}{\left(\dfrac{b'}{t}\right)^{\frac{3}{4}}} & if\ F_{cc} < F_{cy} \\ F_{cy} & otherwise \end{cases}$$

$$W_e = 1.7\ t\ \sqrt{\frac{E_{cc}}{F_{cc}}}$$

Where b' is the sum of length of each 'L' section of stiffener and t is the thickness. The value of C_e is a constant that can be obtained based on the edge condition of each 'L' section in a stiffener. Table below shows an example of edge condition and C_e values for different materials.

Table 4.Edge condition for Aluminium and Steel with its corresponding C_e values

Material	Edge condition	C_e

Aluminium	2 free edges	0.295
	1 free edge	0.317
	No free edges	0.339
Steel	2 free edges	0.274
	1 free edge	0.318
	No free edges	0.362

Hat-shaped stiffener:

Total area (mm^2)	110
Calculated critical crippling stress, F_{cc} (Gpa)	0.5298
Effective width, W_e (mm)	45.2

Front spar cap:

Total area (mm^2)	66
Calculated critical crippling stress, F_{cc} (Gpa)	0.3705
Effective width, W_e (mm)	42.1

Rear spar cap:

Total area (mm^2)	44
Calculated critical crippling stress, F_{cc} (Gpa)	0.3705
Effective width, W_e (mm)	22.6

Notice that in the tables above, all the calculated critical crippling stresses, F_{cc} are higher than the values of F_{cy}. Hence the F_{cc} for all stiffeners are evaluated as the second case in the F_{cc} equation where F_{cc} = F_{cy}.

For all stiffeners:

$$F_{cc} = F_{cy} = 276\ Mpa$$

2.8 SKIN PANEL LOCAL BUCKLING STRESS AND LOAD

By using the compressible buckling formula (Eq. 1) shown previously, the skin panel buckling for each section can be calculated since all the parameters are known. The results are shown in the table below

Table 5.Critical Stresses and Loads for Skin Panel

Skin Panel	**Skin panel critical buckling stress, F_{sk} (MPa)**	**Critical buckling load per unit length, $N_{lim,skin}(N/mm)$**
1	5.44	6.1652
2	9.2367	13.0185
3	5.8919	7.5965

4	13.338	18.4908
5	4.1632	4.7179
6	22.485	39.2076
7	4.3042	4.9009
8	13.372	18.5478
9	5.8876	7.5899
10	9.2555	13.0506
11	5.4854	6.2240
12	129.529	366.1036

In this analysis, the local buckling stress for stiffener did not have to be calculated since in Eq. 1, the 'b' parameter which is the length of the loaded edge is far smaller (by the first order of magnitude) for the stiffener compared to the skin which results in a large magnitude of buckling stress that does not concern our analysis to find the critical minimum.

2.8.1 COMBINED SKIN AND STIFFENERS CRIPPLING STRESS, LIMIT AND ULTIMATE CRIPPLING LOAD PER UNIT LENGTH

In order to determine the limit and ultimate load for the combined stiffener and skin material, the critical crippling force, P_{cc} needs to be calculated from the critical crippling stress, F_{cc} and the effective area of the combined material. The formula is given as shown below:

$$P_{cc} = F_{cc} \times Area_{effective}$$

$$Area_{effective} = W_e \times t_{skin} + Area_{stiffener}$$

Once the critical crippling forces are found, the ultimate crippling force per unit length of the material can be calculated. It will be the value of stress where the combined skin and stiffener will cripple under such loading condition.

$$N_{ult,cc} = \frac{P_{cc}}{b}$$

Where b is the distance between stiffeners.

By applying a factor of safety 1.5, the limit load per unit length is:

$$N_{lim,cc} = \frac{N_{ult,cc}}{1.5}$$

Notice that the above equation is a rearrangement of equation 2.5.1 shown previously

Table 6. Critical Crippling Load, Ultimate and Limit Load per Unit Length

Panel	$\boldsymbol{P_{cc}\ (kN)}$	$\boldsymbol{N_{ult,cc}(N/mm)}$	$\boldsymbol{N_{lim,cc}\ (N/mm)}$
1	1.720	71.6	47.73
2	4.047	219.5	146.3

3	4.047	175.3	116.9
4	4.047	263.8	175.8
5	2.765	100.7	67.11
6	4.047	342.5	228.3
7	4.047	149.8	99.89
8	2.765	180.4	120.3
9	4.047	175.2	116.8
10	4.047	219.7	146.5
11	4.047	169.2	112.8
12	1.720	142.0	94.65

2.8.2 Solve for the internal stresses (bending and shear) in each section

The figure below represents the direction of shear flow in the panel and the direction of torque in each wing box.

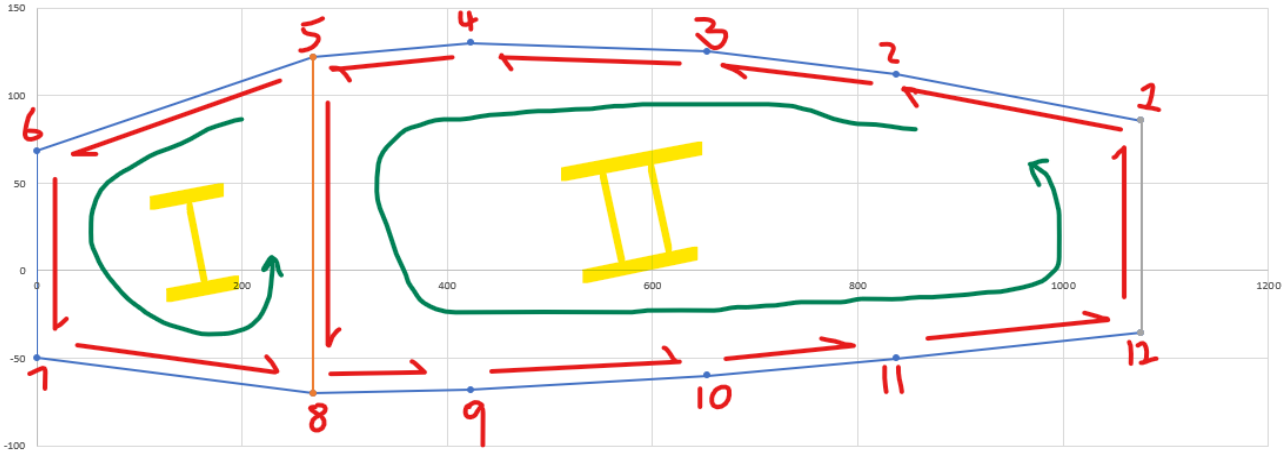

Figure 35. Idealised Cross-section with direction of Internal Shear and Torque

Firstly, the area of each boom was calculated using

$$B = \sum A_{panel} + A_{stiffener}$$

The centroid of the cross section was then found using the equations

$$\overline{x} = \frac{\sum B_i \cdot x_i}{\sum x_i}$$

This boom area is then used to find the second Moment of Area, I_{xx} and I_{yy}

$$I_{xx} = \sum B \cdot (y_i - \overline{y})^2$$

$$I_{yy} = \sum B \cdot (x_i - \overline{x})^2$$

To find the shear flow on each panel, one panel on each wing box was cut open to begin calculations. From here, the basic shear flows for each panel were calculated.

$$q_{b,i} = -\frac{S_y}{I_{xx}} B_i \cdot y_i + q_{b,i-1}$$

Due to the assumption of the open wing box,

$$q_{12} = 0 \ \ \& q_{34} = 0$$

The panel Aspect Ratios were determined, and the rate of twist equations were formed, one for each wing box

$$\left(\frac{d\theta}{dz}\right)_R = \frac{1}{2A_R G}\oint_R q_s \frac{ds}{t} = \frac{1}{2A_R G}\oint_R \left(q_b + q_{s,0,R}\right)\frac{ds}{t}$$

To obtain the third equation in order to obtain the values for Constant shear flows, $q_{s,0,R}$, the internal and external torques were equated. The location of the torque centre was set to be at the centre of the Front spar to simplify further calculations

$$S_y \xi_x = \sum p_i q_{b,i} ds + \sum 2A_R q_{s,0,R}$$

Where

ξ_x=Distance between applied shear force and Front spar

A_R= Area of wing box.

Solving these three equations simultaneously, the Constant shear flows are determined and are added to the basic shear flow to get the Total Shear flows on each panel. The shear stresses in each panel is obtained by dividing the respective shear flows with the thickness of the panel.

$$\tau = \frac{q}{t}$$

The bending stress is given by the equation

$$\sigma = \frac{M_x y}{I_{xx}}$$

The tables below summarise the Shear Stresses and the Bending Stresses on each panel for the load cases: flight cruising at ceiling, taxing before take-off and take off.

Table 7. Internal Stresses for Steady Cruise Flight at Brace

Skin panel	Shear Stress (MPa)	Bending Stress (MPa)
$1 \rightarrow 2$	-5.127	-43.648
$2 \rightarrow 3$	4.905	-62.422
$3 \rightarrow 4$	5.461	-71.713
$4 \rightarrow 5$	5.214	-75.286
$5 \rightarrow 6$	-1.239	-69.569
$6 \rightarrow 7$	2.875	-31.229
$7 \rightarrow 8$	-1.750	53.217
$8 \rightarrow 9$	5.575	67.642
$9 \rightarrow 10$	-2.716	66.213
$10 \rightarrow 11$	-4.222	60.496
$11 \rightarrow 12$	-3.411	53.349
$12 \rightarrow 1$	-3.384	42.928

Table 8. Internal Stresses for Take Off at Brace

Skin panel	Shear Stress (MPa)	Bending Stress (MPa)
$1 \rightarrow 2$	-5.512	-46.923
$2 \rightarrow 3$	5.273	-67.106
$3 \rightarrow 4$	5.870	-77.093
$4 \rightarrow 5$	5.605	-80.935
$5 \rightarrow 6$	-1.332	-74.789
$6 \rightarrow 7$	3.090	-33.573
$7 \rightarrow 8$	-1.882	57.211
$8 \rightarrow 9$	5.994	72.717

$9 \rightarrow 10$	2.920	71.181
$10 \rightarrow 11$	4.539	65.035
$11 \rightarrow 12$	-3.667	57.352
$12 \rightarrow 1$	-3.638	46.149

Table 9. Internal Stresses for Taxiing at Brace

Skin panel	Shear Stress (MPa)	Bending Stress (MPa)
$1 \rightarrow 2$	3.621	16.699
$2 \rightarrow 3$	-3.464	23.882
$3 \rightarrow 4$	-3.856	27.436
$4 \rightarrow 5$	-3.682	28.803
$5 \rightarrow 6$	0.875	26.616
$6 \rightarrow 7$	-2.03	11.948
$7 \rightarrow 8$	1.236	-20.360
$8 \rightarrow 9$	-3.937	-25.879
$9 \rightarrow 10$	1.918	-25.332
$10 \rightarrow 11$	2.982	-23.145
$11 \rightarrow 12$	2.409	-20.410
$12 \rightarrow 1$	2.390	-16.423

2.8.3 Determine a margin of safety for each section component for Yielding, Buckling and Crippling

Margin of safety is an indicator of the system's additional capacity to carry load and stress, given by the following equation:

$$Margin\ of\ safety = \frac{Load_{allowable}}{Load_{applied}} - 1$$

Cruising condition:

Table 10. Buckling Margin of Safety for Skin Panel during Cruising

Skin Panel	Compression bending stress $(\boldsymbol{MPa})$	Critical skin buckling $(\boldsymbol{MPa})$	Margin of safety (buckling)
$1 \rightarrow 2$	43.648	5.44	-0.7887
$2 \rightarrow 3$	62.422	9.2367	-0.7492
$3 \rightarrow 4$	71.713	5.8919	-0.8607
$4 \rightarrow 5$	75.286	13.338	-0.6997
$5 \rightarrow 6$	69.569	4.1632	-0.8985
$6 \rightarrow 7$	31.229	22.485	0.2202

Table 11. Yielding Margin of Safety for Skin and Stiffener during Cruising

Effective skin and stiffener	Compression bending stress (MPa)	Compressive yield strength (MPa)	Margin of safety (yielding)
1	43.648	276	9.716
2	62.422	276	6.493
3	71.713	276	5.522
4	75.286	276	5.212
5	69.569	276	5.723
6	31.229	276	13.97

Table 12. Crippling Margin of Safety for Skin and Stiffener during Cruising

Effective skin and stiffener	Compression bending stress (MPa)	Critical crippling stress (MPa)	Margin of safety (crippling)
1	43.648	370.5	14.385
2	62.422	529.8	14.383
3	71.713	529.8	12.520
4	75.286	529.8	11.926
5	69.569	529.8	12.906
6	31.229	529.8	20.106

Take-off condition:

Table 13. Buckling Margin of Safety for Skin Panel during Take-off

Skin Panel	Compression bending stress (MPa)	Critical skin buckling (MPa)	Margin of safety (buckling)
$1 \rightarrow 2$	46.923	5.44	-0.8840
$2 \rightarrow 3$	67.106	9.2367	-0.8623
$3 \rightarrow 4$	77.093	5.8919	-0.9235
$4 \rightarrow 5$	80.935	13.338	-0.8352
$5 \rightarrow 6$	74.789	4.1632	-0.9443
$6 \rightarrow 7$	33.573	22.485	-0.3302

Table 14. Yielding Margin of Safety for Skin and Stiffener during Take-off

Effective skin and stiffener	Compression bending stress (MPa)	Compressive yield strength (MPa)	Margin of safety (yielding)
1	46.923	276	4.8819
2	67.106	276	3.1128
3	77.093	276	2.5800
4	80.935	276	2.4101
5	74.789	276	2.6903
6	33.573	276	7.2208

Table 15. Crippling margin of Safety for Skin and Stiffener during Take-off

Effective skin and stiffener	Compression bending stress (MPa)	Critical crippling stress (MPa)	Margin of safety (crippling)
1	46.923	370.5	7.8959
2	67.106	529.8	7.8949
3	77.093	529.8	6.8722
4	80.935	529.8	6.5459
5	74.789	529.8	7.0839
6	33.573	529.8	11.035

Taxiing condition:

Table 16. Buckling Margin of Safety for Skin Panel during Taxi

Skin Panel	Compression bending stress (MPa)	Critical skin buckling (MPa)	Margin of safety (buckling)
$7 \rightarrow 8$	20.36	4.3042	-0.7885
$8 \rightarrow 9$	25.879	13.372	-0.4832
$9 \rightarrow 10$	25.332	5.8876	-0.7675
$10 \rightarrow 11$	23.145	9.2555	-0.6001
$11 \rightarrow 12$	20.41	5.4854	-0.7312
$12 \rightarrow 1$	16.423	129.529	6.8870

Table 17. Yielding Margin of Safety for Skin and Stiffener during Taxi

Effective skin and stiffener	Compression bending stress (MPa)	Compressive yield strength (MPa)	Margin of safety (yielding)
7	20.36	276	12.555
8	25.879	276	9.6650
9	25.332	276	9.8953
10	23.145	276	10.924
11	20.41	276	12.522
12	16.423	276	15.805

Table 18. Crippling margin of Safety for Skin and Stiffener during Taxi

Effective skin and stiffener	Compression bending stress (MPa)	Critical crippling stress (MPa)	Margin of safety (crippling)
7	20.36	370.5	17.197
8	25.879	529.8	19.472
9	25.332	529.8	19.914
10	23.145	529.8	21.890
11	20.41	529.8	24.957
12	16.423	529.8	21.559

2.9 Estimate the fatigue life of the component using S-N curves.

The Fatigue life of the component can be approximated using an S-N curve for aluminium 2024-T3. The curve used the fatigue life analysis is illustrated in Figure 36 below.

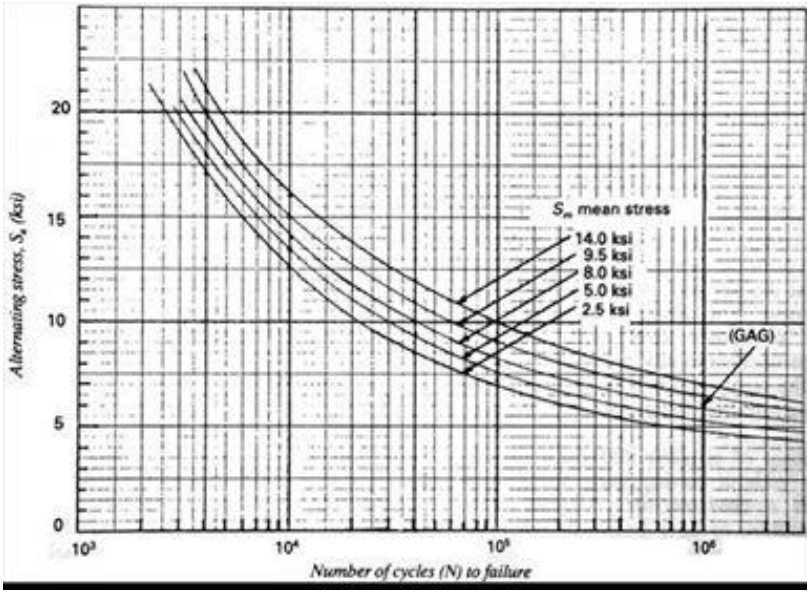

Figure 36. S-N curve for AL2024-T3

Generally, analysis using S-N curves requires detailed data on the ground and flight loading of an aircraft during flights including the maximum and mean stresses experienced. An example this data is shown in Figure 37 below.

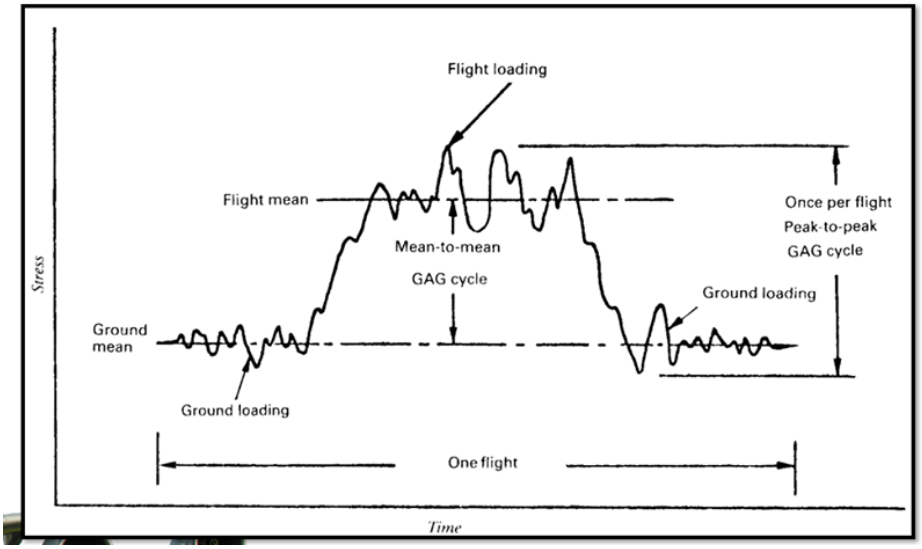

Figure 37. Stress Oscillation vs Time Sample

These data were not available for the analysis and the calculated stress distribution in the idealised wing section is used instead as an approximation. Significant amount of inaccuracies is predicted in the estimated fatigue life of the aircraft as the calculation will be based on an idealised structure under approximated loadings. For this approximation of the fatigue life of the aircraft, the average of the bending stresses calculated are used as the mean stress and the maximum calculated bending stress is approximated as the alternating stress amplitude. The values used for the fatigue life calculation are recorded in Table 19 below.

Table 19. Mean and Alternating Stresses for Different Load Cases

	Load Cases		
	Taxiing	Take Off	Cruise
Mean Stress (kis)	3.179934	9.195868	8.554027
Alternating Stress Amplitude (ksi)	3.753438	11.73865	10.91933

Since the mean stress for all three loading conditions lies between the available mean stress curves, the number of cycles to failure for the upper and lower limits of each case is obtained and interpolated to produce the number of cycle to failure at the specified mean stresses. An example calculation for the take-off case is detailed below.

$$N_{8\ ksi} = 3 \times 10^4$$

$$N_{9.5\ ksi} = 4 \times 10^4$$

$$N_{9.2\ ksi} = \frac{9.2 - 8}{9.5 - 8}(4 \times 10^4 - 3 \times 10^4) + 3 \times 10^4$$

$$N_{Take\ off,9.2\ ksi} = 3.8 \times 10^4$$

The cycles to failure for the cruising case can be calculated with the same method.

$$N_{Cruising,8.6\ ksi} = 3.4 \times 10^4$$

The calculated cycles to failure is summarised in Table 20 below.

Table 20. Cycles to Failure for Different Load Cases

	Load Cases		
	Taxiing	Take Off	Cruising
Number of Cycles to failure	N/A	3.8×10^4	3.4×10^4

3 Discussion

The shear force and bending moment analysis on the aircraft's wings shows a general trend of increasing bending stress from the tip to the root of the wing, with maximum stresses occurring at the joint to the brace in the cruising case and at the root of the wing under grounded loading conditions. This effectively demonstrates the bending moment distribution illustrated in Figure 19 and Figure 21 where the bending moment is maximum at the corresponding points. The brace of the aircraft therefore effectively directs the maximum bending stress away from the joint of the wing during flight, which should improve the structural integrity of the aircraft. The brace support also effectively keeps the shear force over the wing section relatively constant across its span in both cruising and ground conditions as illustrated in Figure 18 and Figure 20

The stress analysis over the idealized wing section shows variations in the bending and shear stresses around the surface of the airfoil, with maximum bending and shear stresses occurring around boom 5 and 8. This trend is consistent with theoretical predictions as these locations corresponds with the front spar where the bending moment and shear force is expected to be maximum.

The bending stress distribution across the idealized wing section produced values that are significantly smaller than the compressive yield strength and critical crippling stress of 2024-T3 Aluminium, but higher than the critical buckling stresses. The skin on the aircraft's wings is therefore expected to buckle during ground, takeoff and cruising conditions, with buckling expected to be maximum during take-off and minimum while the airplane is on the ground. Preventative measures could be taken to reduce the buckling of the aircraft including the installation of additional stiffeners or by increasing the skin thickness of the wings. However, both solutions introduce additional weight to the aircraft's architecture and may affect its performance.

Based on rough estimation using the S-N curve, the aircraft is expected to fail due to fatigue after 3.8×10^4 cycles under take-off conditions and 3.4×10^4 cycles during cruising. A fatigue life was not calculated for the aircraft under taxiing conditions as the calculated alternating stress amplitude does not coincide with the corresponding mean stress curve. These calculations are expected to contain a large error margin as the values used are based on idealised model of the wing and uses an inaccurate estimate of the alternating stress amplitude and mean stress, due to the lack of information available on the Cessna 172. The accuracy of the fatigue life calculation can be increased significantly if the measured oscillating stress data during the aircraft's flight is available.

Overall, the trends observed in the calculated stresses are consistent with the corresponding solid mechanic principles, but the analysis lacks accuracy overall as large amount of assumptions were made due to the lack of official information. More detailed analysis is necessary to produce an accurate analysis on the stress distribution and fatigue lifetime of the Cessna 172.

4 Conclusion

Analysis on the wings of the Cessna 172 was successful with the calculated values agreeing with the underlying solid mechanical principles. The results demonstrate the effectiveness of the brace and offers an approximation of the bending and shear stress distribution over a section of the aircraft's wings. The fatigue life calculations estimate the cycles to failure number of 3.8×10^4 *and* 3.4×10^4 for the plane's wings under take-off and cruising load conditions respectively. The fatigue life of the wings under taxiing load conditions were not able to be calculated. Overall, the analysis of the wings of the Cessna 172 lacks accuracy as many assumptions and simplifications were required due to the lack of official data on the aircraft. The fatigue life calculated in this report is likely extremely inaccurate as the stress oscillation data of aircraft during flight is unavailable and rough approximations of the required values are used instead.

Bibliography

[1] Wikipedia, "Cessna 172," [Online]. Available: https://en.wikipedia.org/wiki/Cessna_172. [Accessed 28 04 2020].

[2] K. Wichita, Cessna 100 Series Service Manual, 1968.

[3] "aviationchief," [Online]. Available: http://www.aviationchief.com/operating-flight-strength-v-g--v-n-diagrams.html. [Accessed 28 04 2020].

[4] "Airfoil tools," [Online]. Available: http://airfoiltools.com/. [Accessed 28 04 2020].